AGU PUBLICATIONS

JGR

Journal of Geophysical Research: Atmospheres

RESEARCH ARTICLE
10.1002/2015JD024254

# Troposphere-stratosphere dynamical coupling in the southern high latitudes and its linkage to the Amundsen Sea

**Mark R. England[1], Tiffany A. Shaw[2], and Lorenzo M. Polvani[1,3]**

[1]Department of Applied Physics and Applied Mathematics, Columbia University, New York, New York, USA, [2]Department of the Geophysical Sciences, University of Chicago, Illinois, Chicago, USA, [3]Department of Earth and Environmental Science, Lamont-Doherty Earth Observatory, Columbia University, New York, New York, USA

**Key Points:**
- Extreme stratospheric heat flux events are linked to significant longitudinal shifts in the Amundsen Sea Low
- Stratospheric heat flux index can be used to evaluate CMIP5 models
- A degraded stratosphere is linked to reduced mean sea level pressure variability over the Antarctic Peninsula

**Correspondence to:**
M. R. England,
mre2126@columbia.edu

**Citation:**
England, M. R., T. A. Shaw, and L. M. Polvani (2016), Troposphere-stratosphere dynamical coupling in the Southern high latitudes and its linkage to the Amundsen Sea, *J. Geophys. Res. Atmos.*, *121*, 3776–3789, doi:10.1002/2015JD024254.

Received 24 SEP 2015
Accepted 31 MAR 2016
Accepted article online 6 APR 2016
Published online 21 APR 2016



**Abstract** Extremes in the distribution of Southern Hemisphere stratospheric heat flux are connected simultaneously to anomalous high-latitude tropospheric weather patterns in reanalysis, consistent with results from the Northern Hemisphere. The dynamical links are revealed using a metric based on extreme stratospheric planetary-scale wave heat flux events, defined as the 10th and 90th percentiles of the daily high-latitude wave 1 heat flux distribution at 50 hPa. We show extreme negative (positive) heat flux events are linked to a westward (eastward) shift in the Amundsen Sea Low and anomalous warming (cooling) over the Amundsen Bellingshausen Seas in reanalysis data. Since coupling to the stratosphere via planetary waves has significant impacts on the tropospheric circulation of both hemispheres, it is important to understand which coupled climate models can reproduce this phenomenon. The heat flux metric is used to evaluate troposphere-stratosphere coupling in models participating in the Coupled Model Intercomparison Project Phase 5 (CMIP5) and compare their performance across hemispheres. The results show that models with a degraded representation of stratospheric extremes exhibit robust biases in tropospheric sea level pressure variability over the Antarctic Peninsula. Models which fail to capture the extremes in stratospheric heat flux, significantly underestimate the variance of the distribution of mean sea level pressure anomalies over Western Antarctica.

## 1. Introduction

Variability in the stratosphere is closely linked to anomalous tropospheric weather patterns in the Southern Hemisphere (SH) [*Gerber et al.*, 2012; *Kidston et al.*, 2015]. Coupling mainly occurs in SH spring time, when the breakdown of the stratospheric vortex influences the position of the tropospheric jet [*Randel*, 1988; *Baldwin and Dunkerton*, 2001; *Baldwin et al.*, 2003; *Gerber et al.*, 2012]. Planetary-scale waves, generated in the troposphere, represent one of the main modes of stratosphere troposphere coupling [*Andrews et al.*, 1987; *Plumb*, 2010] and has significant impacts on the variability of the stratospheric polar vortex [*Polvani and Waugh*, 2004; *Dunn-Sigouin and Shaw*, 2015].

The primary mode of planetary wave coupling is upward wave coupling where signals in the troposphere propagate up into the stratosphere. *Randel* [1987] found that wave 1 exhibits an upward vertical propagation time scale of 4 days between the middle troposphere and the middle stratosphere and that its vertical structure is significantly different from waves 2 and 3. The upward propagation involves significant transfers of heat and momentum poleward [*van Loon and Jenne*, 1972; *Randel*, 1988]. *Shaw et al.* [2010] demonstrate that in addition to the upward coupling, wave 1 exhibits downward wave coupling (wave pattern in the stratosphere leads wave pattern in the troposphere with a propagation timescale around 5 days) from September to December when the zonal flow exhibits a bounded wave geometry. Over the past several decades, ozone depletion has increased downward wave coupling during November and December because the bounded wave geometry extends later into the year in reanalysis data and models [*Harnik et al.*, 2011; *Shaw et al.*, 2011].

Planetary wave coupling has a significant impact on the tropospheric circulation in the Northern Hemisphere (NH), associated with a distinct regional signal in the North Atlantic basin [*Shaw et al.*, 2014] (subsequently referred to as S14). The tropospheric impact was revealed using an index based on extreme values of the high-latitude heat flux at 50 hPa. The eddy heat flux is proportional to the vertical group velocity according to linear wave theory and is thus a measure of vertical coupling. Large positive eddy heat fluxes, indicating upward wave coupling, were simultaneously associated with anomalous high pressure over the North Atlantic reminiscent of the negative phase of the NAO whereas large negative eddy heat flux, indicating downward

wave coupling, involved opposite signed patterns. The simultaneous relationship reflected the peak time in the life cycle of planetary wave events in the stratosphere [see *Dunn-Sigouin and Shaw*, 2015, Figure 2]. S14 used the heat flux index to show that models with a biased stratospheric eddy heat flux distribution exhibited biases in eddy geopotential height and jet stream position in the North Atlantic troposphere. The models with the largest stratospheric heat flux bias were all low top, following the definition of *Charlton-Perez et al.* [2013].

We investigate whether planetary wave coupling has a significant regional signature in the SH. One of the most important zonally asymmetric features in the SH is the Amundsen Sea Low (ASL). The ASL, a low-pressure center located in the region 60–75°S, 170–290°E, is a key driver of circulation variability over West Antarctica and has a large impact on the sea ice extent in surrounding regions [*Turner et al.*, 1997; *Hosking et al.*, 2013]. The formation of the ASL is attributable to a combination of (i) flow separation over the coastal line of the Ross Sea embayment and the steep orography inland [*Baines and Fraedrich*, 1989] and (ii) the strong baroclinicity resulting from the irregular coastline of Antarctica, which intensifies the cyclogenesis patterns in the region [*Walsh et al.*, 2000; *Fogt et al.*, 2012]. It is an essentially barotropic phenomenon, and its climatology is well documented by *Turner et al.* [2013a].

We seek to address the following questions: Are stratospheric heat flux extremes linked to a regional circulation in the troposphere in the SH? What is the impact of the coupling in the Amundsen Sea region? Does troposphere-stratosphere planetary wave coupling play as dominant a role in setting the mean state and variability of the tropospheric circulation as it does in the NH? Can tropospheric biases in the Amundsen Sea region in CMIP5 models be linked to the ability to represent extreme stratospheric heat flux events?

This paper is organized as follows. Section 2 describes the reanalysis data set and CMIP5 simulations analyzed in this study. In section 3 the links between stratospheric planetary-scale wave heat flux extremes and SH tropospheric weather and climate patterns in reanalysis data are examined. In section 4 the representation of stratospheric heat flux extremes in CMIP5 models is studied, and coupling with the tropospheric circulation is compared in models with large and small biases in stratospheric heat flux extremes. Section 5 concludes the paper with a summary and discussion.

## 2. Data and Methods

This study uses daily data from the European Centre for Medium-Range Weather Forecasts (ECMWF) Interim (ERA-Interim) reanalysis for the years 1979–2005 [*Dee et al.*, 2011]. In addition, we make use of daily and monthly data from 30 CMIP5 historical simulations (Table 1) [*Taylor et al.*, 2012]. In this study anomalies are computed by removing the climatological seasonal cycle (1979–2005).

The following analysis is based on the daily wave 1 (meridional) heat flux, i.e., $\overline{v'T'}_{k=1}$ at 50 hPa where the overbar represents a zonal average, the prime indicates a deviation from the zonal average, and $k$ is the zonal wave number, which is extracted using Fourier decomposition. We use the wave 1 heat flux, which represents 80% of the eddy (deviation from the zonal mean) heat flux variability, as a measure of vertical wave coupling [*Charney and Drazin*, 1961]. The 50 hPa level, located in the mid to lower region of the stratosphere, is chosen because it is a standard output level in the ERA-Interim and CMIP5 data sets. The wave 1 heat flux is averaged between 60° and 90°S creating a daily time series, which is hereafter referred to as the high-latitude stratospheric heat flux. This latitudinal band is where the temporal variability of the heat flux is maximum. The sensitivity of the results to the choice of latitudinal average and the effect of weighting by the cosine of the latitude are negligible.

The study focuses on September, October, and November (SON), which is the period of maximum wave coupling between the troposphere and stratosphere in the SH (Figure 1a, blue) [*Shaw et al.*, 2010]. S14 analyzed the period January, February, and March (JFM), the period of maximum wave coupling in the NH (Figure 1a, red).

The eddy field is found by calculating the deviation from the zonal mean. The eddy field is broken down into its components of different wave numbers using Fourier decomposition.

## 3. Links Between Stratospheric Wave 1 Heat Flux Extremes and the Tropospheric Circulation in Reanalysis Data

The daily distributions of high-latitude wave 1 heat flux at 50 hPa for both the NH (averaged 60° to 90°N, JFM) in red and the SH (averaged 60° to 90°S, SON) in blue are shown in Figure 1b. Note that the NH distribution

**Table 1.** CMIP5 Historical Data Used in This Study Model Ensemble

| Model | Ensemble member |
|---|---|
| bcc-csm1-1 | r1i1p1 |
| bcc-csm1-1-m[a] | r1i1p1 |
| BNU-ESM | r1i1p1 |
| CanESM2 | r1i1p1 |
| CCSM4 | r1i1p1 |
| CMCC-CESM | r1i1p1 |
| CMCC-CM | r1i1p1 |
| CNRM-CM5[b] | r1i1p1 |
| FGOALS-g2[b] | r1i1p1 |
| FGOALS-s2 | r1i1p1 |
| GFDL-ESM2G[b] | r1i1p1 |
| GFDL-ESM2M[b] | r1i1p1 |
| HadCM3[b] | r1i1p1 |
| inmcm4[b] | r1i1p1 |
| MIROC5 | r1i1p1 |
| NorESM1-M[a] | r1i1p1 |
| CESM1-WACCM | r1i1p1 |
| CMCC-CMS[a] | r1i1p1 |
| GFDL-CM3 | r1i1p1 |
| HadGEM2-CC | r1i1p1 |
| IPSL-CM5A-LR[a] | r1i1p1 |
| IPSL-CM5A-MR[a] | r1i1p1 |
| MIROC-ESM[b] | r1i1p1 |
| MIROC-ESM-CHEM | r1i1p1 |
| MPI-ESM-LR | r1i1p1 |
| MPI-ESM-MR[a] | r1i1p1 |
| MPI-ESM-P | r1i1p1 |
| MRI-CGCM3[a] | r1i1p1 |

[a]Models included in the small bias ensemble.
[b]Models included in the large bias ensemble.

has been multiplied by −1 so that the mean has been flipped from positive to negative, to allow for an easy comparison of the phenomenon in the two hemispheres. In the SH (NH) the mean is negative (positive) meridional heat flux values, consistent with upward propagating waves. The SH wave 1 heat flux distribution has a smaller mean and standard deviation than that of the NH, consistent with the SH having a weaker wave source. The NH wave 1 heat flux distribution therefore has thicker tails; the 10th percentile is 41.7 K $ms^{-1}$ compared to −32.5 K $ms^{-1}$ for the SH, and the 90th percentiles is of −10.8 K $ms^{-1}$ and 4.3 K $ms^{-1}$ for the SH.

From now on we will focus on the SH, and any mention of the heat flux distribution refers to that in the SH. The mean of the distribution is negative and equal to −11.7 K $ms^{-1}$, indicating upward propagation. The standard deviation is equal to 17.2 K $ms^{-1}$. Days with stratospheric heat flux lower than the 10th percentile of the distribution (−432.5 K $ms^{-1}$) will be labeled as "extreme negative heat flux days" and days with values larger than the 90th percentile of the distribution (4.3 K $ms^{-1}$) will be labeled as "extreme positive heat flux days." According to linear wave theory, extreme negative days are associated with upward wave propagation, and extreme positive days are associated with downward wave coupling. As mentioned in section 1, our eddy heat flux index exploits the near-simultaneous stratospheric and tropospheric signals seen in the planetary wave life cycle.

We assess the link between extreme stratospheric heat flux events and the troposphere by comparing the climatological pattern to the patterns during extreme stratospheric events. The climatology of the mean sea

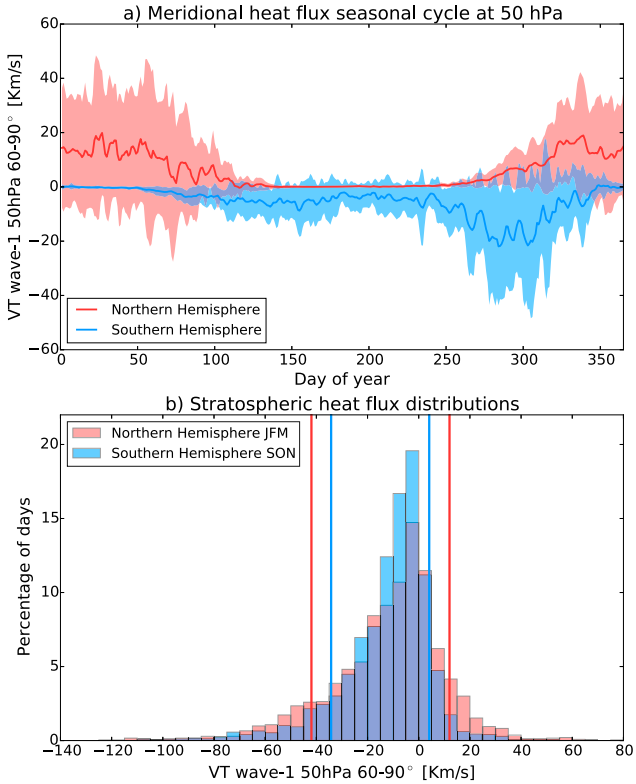


**Figure 1.** The 60°–90°S and 60°–90°N wave 1 meridional heat flux at 50 hPa in ERA-Interim for 1979–2005. (a) Seasonal cycle in both hemispheres. The line shows the mean value of the heat flux, and the shaded envelope gives one standard deviation interval either side. (b) Daily distribution averaged 60°–90°S during SON and 60°–90°N during JFM from 1979 to 2005. The distribution from the NH has been multiplied by −1. The vertical lines represent the 10th and 90th percentiles of the distributions.

level pressure (mslp) from ERA-Interim during SON is shown in Figure 2a from the years 1979–2005. The location and depth of the ASL is indicated in red, in agreement with Figure 1 of *Turner et al.* [2013a]. Figures 2b and 2c show mslp for composites of extreme negative and positive stratospheric heat flux events, respectively. During extreme negative events the ASL center migrates westward by 12°, whereas during extreme positive events it shifts eastward by 32°. This is a significant longitudinal change given the amplitude of the seasonal cycle (taking monthly mean position) is only 40° [*Turner et al.*, 2013b]. These shifts are in the lowest and highest 20th percentiles of the distribution of monthly ASL longitude positions, respectively. *Hosking et al.* [2013] demonstrate how the longitudinal position of the ASL can have a large impact on sea ice

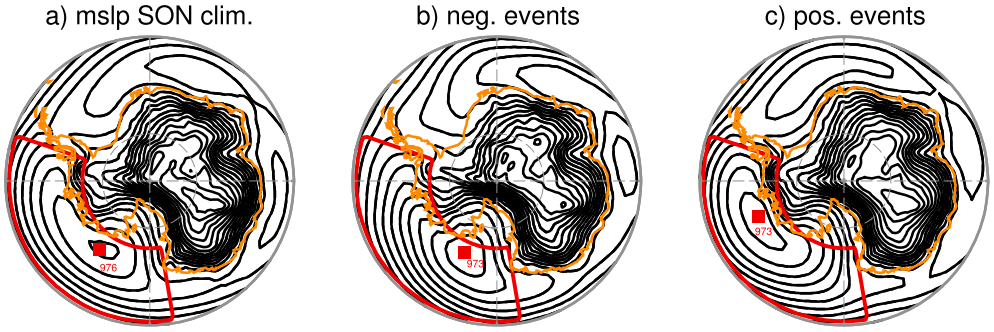


**Figure 2.** The ERA-Interim mean sea level pressure (a) SON climatology, and a composite of (b) extreme negative and (c) positive heat flux events. See text for definition of extreme positive and negative heat flux events. The contour interval is 2 hPa. The Amundsen Sea region (60–75°S, 170–290°E) is shown by the red box. The location of the ASL (the point with the lowest mean sea level pressure in the region) is represented by the red square, and the ASL central pressure is indicated in hPa.

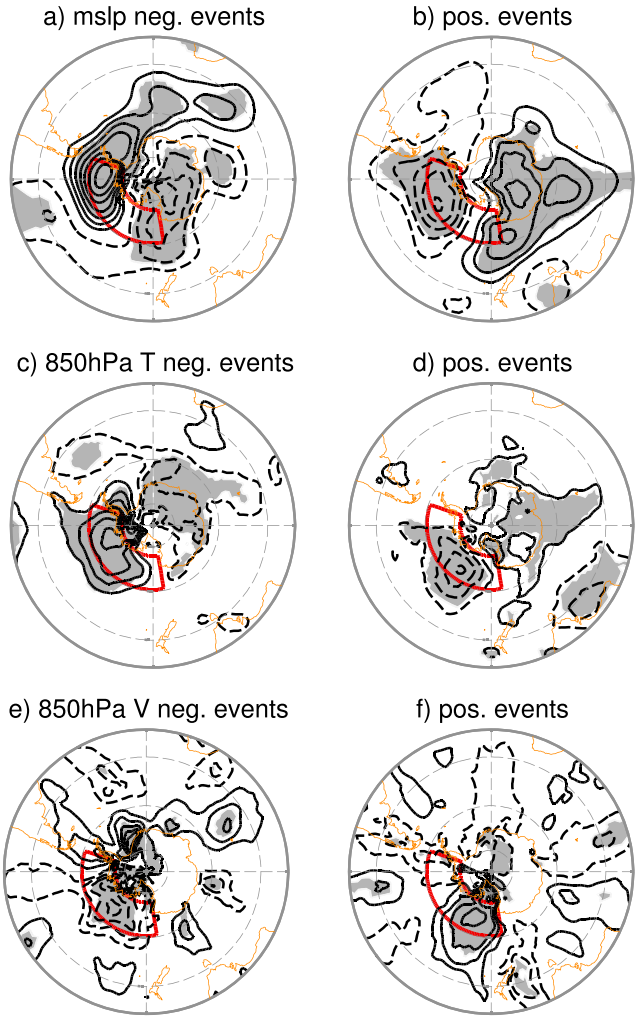


**Figure 3.** ERA-Interim composite of (a, b) mean sea level pressure, (c, d) 850 hPa temperature, and (e, f) 850 hPa meridional wind anomalies during extreme (Figures 3a, 3c, and 3e) negative and (Figures 3b, 3d, and 3f) positive heat flux events. The contour interval is 1 hPa for mean sea level pressure, 0.5 K for temperature, and 0.5 $ms^{-1}$ for the meridional wind. Grey shading shows anomalous values statistically significant at 99% (see Appendix A for details). Black contours show positive values, and dashed contour lines correspond to negative values. The zero contour is omitted. The continents are plotted in brown.

concentration; when the ASL is displaced westward, there is a decrease in sea ice concentration in the Amundsen and Bellingshausen Seas and vice versa.

Figure 3 shows the anomalous mslp (Figures 3a and 3b), anomalous temperature at 850 hPa (Figures 3c and 3d), and anomalous meridional wind (Figures 3e and 3f) during extreme positive and negative heat flux days in SON. During extreme negative heat flux events there is anomalously high mslp over the Bellingshausen Sea, with equatorward flow over the Antarctic Peninsula and strong poleward flow over the Amundsen Sea. Furthermore, there is anomalous warming over the Amundsen and Bellingshausen Seas, due to advection from the northeast (anticyclonic flow around the anomalous high surface pressure). In contrast, for days with extreme positive heat flux values, anomalously low mslp over the Bellingshausen Sea advects cold air from over Antarctica equatorward and westward through cyclonic flow, causing anomalously cold temperatures in this region. These patterns drive the longitudinal movement of the ASL during SON seen in Figure 2.

The stratospheric events are also linked to patterns in the mid troposphere and upper stratosphere. Figure 4 shows the climatalogical 500 hPa (black) and 10 hPa (shaded) wave 1 and anomalous geopotential height, which both exhibit a clear wave 1 structure for composites of extreme negative and positive events. During extreme negative heat flux days (Figures 4b and 4e) geopotential height patterns resemble those near the

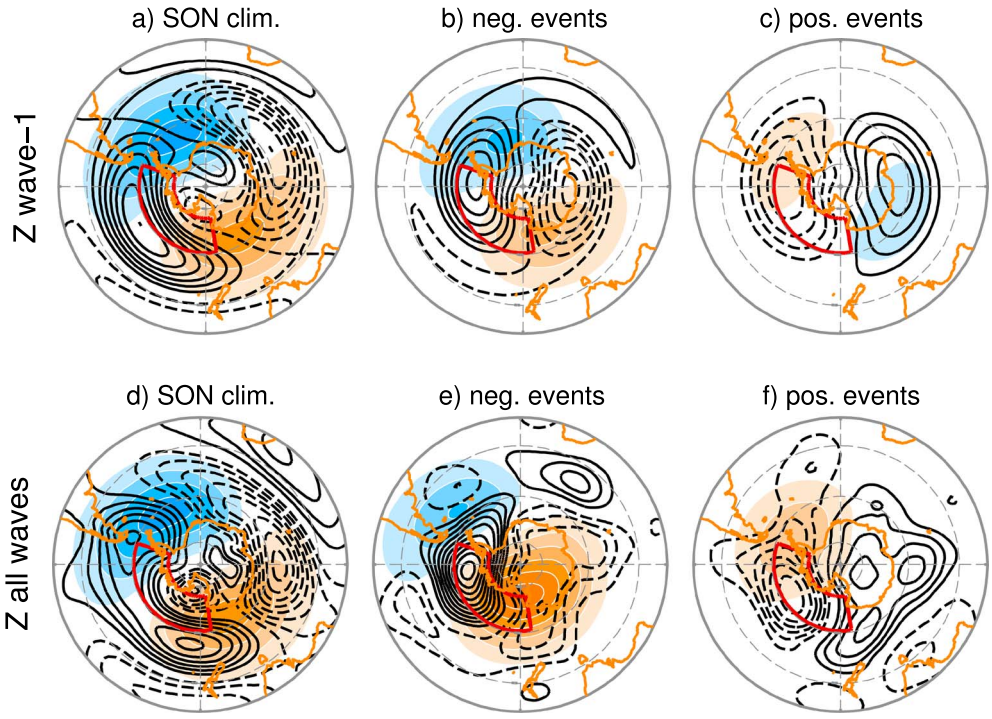


**Figure 4.** The ERA-Interim (a–c) wave 1 and (d–f) eddy geopotential height for (Figures 4a and 4d) SON eddy climatology from 1979 to 2005 and composites of anomalous values for extreme (Figures 4b and 4e) negative and (Figures 4c and 4f) positive heat flux events, at 500 hPa (black) and 10 hPa (shaded). See text for definition of extreme positive and negative heat flux events. Contour interval is 10 m (black) and 100 m (shaded). Black contours and orange shading show positive values, and contour lines and blue shading correspond to negative values. The zero contour is omitted. The continents are plotted in brown, and the Amundsen Sea region is shown in red.

surface but with a westward shift and tend to reinforce the climatology in high latitudes (Figures 4a and 4d). In the troposphere, the wave 1 component (Figure 4b) explains nearly 70% of the anomalous geopotential height pattern in the high latitudes with waves 2 and 3 making up the remainder. The wave pattern between 500 and 10 hPa exhibits a westward phase tilt with height, consistent with upward propagation of wave activity from the troposphere to the stratosphere [*Andrews et al.*, 1987].

During extreme positive heat flux days the geopotential height anomalies are opposite in sign to those during negative heat flux days (Figures 4c and 4f), which moves the ASL eastward (toward the Antarctic Peninsula, Figure 2b). There is an eastward phase tilt with height between 500 and 10 hPa consistent with the idea of wave reflection. Similar to the extreme negative case, wave 1 (Figure 4c) explains roughly 80%. of the anomalous geopotential height pattern (Figure 4f).

These reanalysis results show that extreme variations of the stratospheric wave 1 heat flux are linked to the Amundsen Sea region. The next step is to use the high-latitude heat flux metric to evaluate the representation of stratospheric heat flux events in CMIP5 models including their coupling to the troposphere.

## 4. Links Between Stratospheric Wave 1 Heat Flux Extremes and the Tropospheric Circulation in CMIP5 Models

### 4.1. Representation of Stratospheric Heat Flux Extremes

Here we use the stratospheric heat flux extremes metric to evaluate how well CMIP5 climate models simulate planetary-scale wave coupling between the troposphere and stratosphere. The daily high-latitude heat flux distributions at 50 hPa is calculated for the CMIP5 models listed in Table 1. Figure 5 shows the percentage of days in SON for the years 1979 to 2005 that were classified as extreme negative heat flux days (values less than the 10th percentile of the ERA-Interim distribution, $-34.2$ K ms$^{-1}$) against the percentage of days labeled as extreme positive heat flux days (values greater than the 90th percentile of the ERA-Interim distribution,

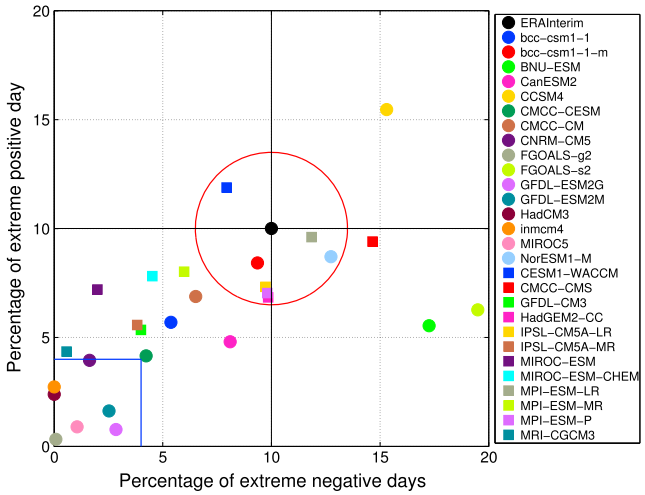


**Figure 5.** Percentage (frequency) of extreme negative wave 1 heat flux events versus extreme positive events at 50 hPa averaged 60°–90°S during SON. Here negative and positive extreme events are defined as the 10th and 90th percentiles of the ERA-Interim distribution for SON 1979 to 2005 with values of $< -34.2$ K ms$^{-1}$ and $> 4.1$ K ms$^{-1}$, respectively. CMIP5 models, with circles representing low-top models and squares representing high-top models, along with the ERA-Interim data are plotted averaged over 1979 to 2005. The blue square is used to define the large bias models, and the red circle is used to define the small bias models.

4.1 K ms$^{-1}$). The models have been color coded in the same manner as S14 with circles representing low-top models and squares showing high-top models, following the definition of *Charlton-Perez et al.* [2013].

The percentage of extreme negative heat flux days and the percentage of extreme positive heat flux days at 50 hPa for the CMIP5 models are significantly correlated ($r = 0.64$, $p = 0.01$). The correlation suggests that models which underpredict the number of extreme positive heat flux days also underpredict the number of extreme negative heat flux days. This is to be expected because downward wave coupling is preceded by upward wave coupling. The majority of CMIP5 models underpredict the stratospheric extremes (both positive and negative) at 50 hPa in the SH (models in the lower left quadrant).

Two model ensembles are constructed based on the bias relative to the 10th and 90th percentiles of the ERA-Interim heat flux distribution. Models are labeled as "small bias" if the combined bias of positive and negative extremes at 50 hPa is less than 3.5% (models contained within red circle of radius 3.5% in Figure 5). Models are labeled as "large bias" if the percentage of either the extreme negative or extreme positive heat flux days is under 4.0% (models contained within blue square in Figure 5). This classification system produces seven small bias models and seven large bias models (Table 2). The results presented below are largely insensitive to the addition or removal of one model from the ensembles.

The distribution of the large bias ensemble is significantly different from the ERA-Interim distribution at 95% significance (compared red and black in Figure 6) whereas the distribution of the small bias ensemble is

**Table 2.** Classification of Models as Small or Large Bias as Indicated by Figure 5[a]

| Small bias model set | Large bias model set |
|---|---|
| bcc-csm1-1-m (L) | CNRM-CM5 (L) |
| NorESM1-M (L) | FGOALS-g2 (L) |
| CMCC-CMS (H) | GFDL-ESM2G (L) |
| IPSL-CM5A-LR (H) | GFDL-ESM2M (L) |
| IPSL-CM5A-MR (H) | HadCM3 (L) |
| MPI-ESM-MR (H) | inmcm4 (L) |
| MRI-CGCM3 (H) | MIROC5 (L) |

[a]Low-top models are shown by (L) and high-top models are shown by (H).

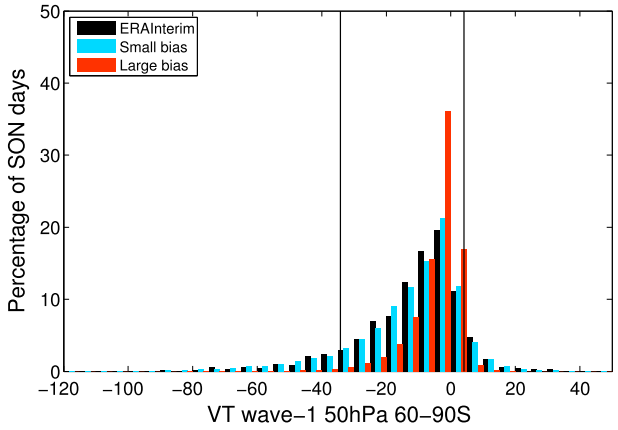


**Figure 6.** Distribution of 50 hPa wave 1 meridional heat flux averaged 60°-90°S during SON from 1979 to 2005 for ERA-Interim (black) and ensemble of CMIP5 models with the small (blue) and large (red) biases relative to ERA-Interim, with model ensembles defined in Table 2. The vertical black lines represent the 10th (−32.5 K $ms^{-1}$) and the 90th (4.3 K $ms^{-1}$) percentile values of the daily ERA-Interim distribution.

significantly similar (compared blue and black in Figure 6), according to a random sampling Kolmogorov-Smirnov test (Table 3). Note that a regular Kolmogorov-Smirnov test was not used because of the known biases introduced into the statistical test when applied to populations of significantly different sizes. The statistical analysis shows that the large bias models do not capture the mean or higher-order moments of the ERA-Interim distribution.

All large bias models are low-top models, consistent with S14's findings in the NH. All six models identified in S14 as large bias for the NH are also part of the large bias model ensemble in the SH. Models which fail to replicate the heat flux extremes at 50 hPa in one hemisphere also underrepresent the extremes in the other hemisphere which seems to imply there are mechanisms intrinsic to these models. Although the majority of the models in the small bias ensemble are high top, two models (bcc-csm-1-m and NorESM1-M) are low top. Only two models (MPI-ESM-MR and MPI-ESM-P) are contained in the small bias model ensembles in both hemispheres. It can be seen from Figure 5 that although high-top models are generally better at capturing the extremes in the heat flux distribution, there are some low-top models which perform well by this criterion and there are some high-top models which do much worse such as HadGEM2-CC and CESM1-WACCM.

The large bias models also underestimate negative and positive heat flux extremes at 10 hPa (not shown), with a tendency of the low-top models to fall above the 1-to-1 line, as found by S14. *Shaw and Perlwitz* [2010], motivated by previous work by *Boville and Cheng* [1988], investigated planetary wave biases associated with low-top models. They found that at 10 hPa, low-top models either underpredict upward wave coupling because of excessive damping or overpredict downward wave coupling due to unphysical wave reflection from the model lid.

Figure 7 compares the error at 10 hPa (defined as the radial distance from the ERA-Interim, for which both types of extreme events occur 10% of the time) in the NH during JFM versus the same bias in the SH during SON. The correlation value between the extremes of CMIP5 in the NH JFM and the SH SON is 0.71, consistent with the idea that a model's performance according to this metric is roughly the same between hemispheres,

**Table 3.** Statistics of the Daily Distribution of Wave 1 Heat Flux Averaged 60° – 90°S at 50 hPa During SON for ERA-Interim Data, the Small Bias Model Set, and the Large Bias Model Set for the Years 1979 – 2005

| | | Mean | SD | 10th Percentile | 90th Percentile | KS test *p* Value |
|---|---|---|---|---|---|---|
| 50 hPa | ERA-Interim | −12.05 | 17.62 | −34.23 | 4.10 | 1.00 |
| | Small bias | −12.39 | 17.81 | −34.50 | 3.17 | > 0.05 |
| | Large bias | −4.51 | 8.13 | −14.89 | 1.17 | < 0.05 (95%) |

The Kolmogorov-Smirnov test is relative to ERA-Interim data. For this run no large bias samples had a KS test *p* value over 0.05 while small bias samples had a KS test *p* value over 0.05 95.4% of the time. This was implemented using method in S14 Appendix A.

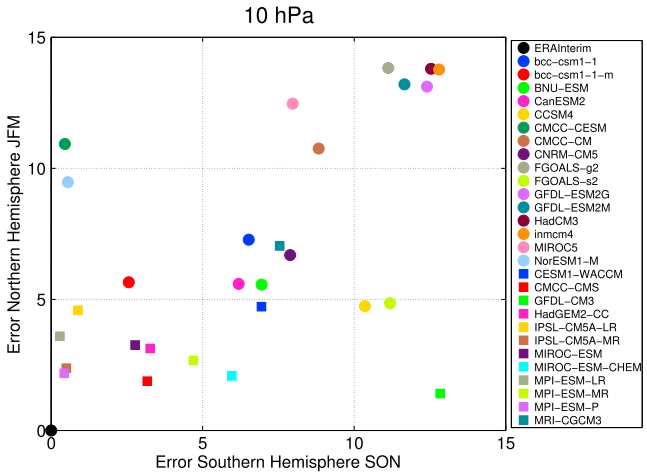


**Figure 7.** Error of the NH JFM high-latitude eddy heat flux versus SH SON high-latitude eddy heat flux at 10 hPa for the CMIP5 models. The error has been defined as the radial distance to ERA-Interim for percentage of extreme negative and positive days ($< -71.34$ K ms$^{-1}$ and $> 2.81$ K ms$^{-1}$ for the SH and $< -10.41$ K ms$^{-1}$ and $> 148.10$ K ms$^{-1}$ for the NH). CMIP5 models, with circles representing low-top models and squares representing high-top models, along with the ERA-Interim data (which has zero error) are plotted.

especially higher up in the stratosphere. The high-top models, in general, are better able to capture the extremes of the planetary wave stratospheric heat flux at 10 hPa in both hemispheres (with the error close to zero in both hemispheres). The low-top models consistently show larger biases in representing the heat flux extremes at 10 hPa. We can see that the majority of models fall on the 1-to-1 line, but with some noticeable exceptions such as GFDL-CM3, a high-top model which performs significantly better at this metric at 10 hPa in the NH, and vice versa for the low-top model CMCC-CESM.

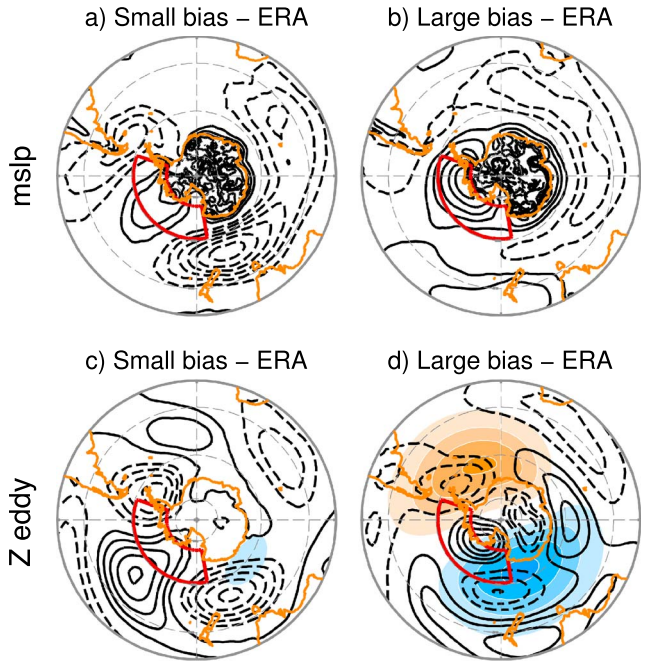


**Figure 8.** Difference in (a, b) climatological mean sea level pressure and (c, d) eddy geopotential height at 500 hPa (black) and 10 hPa (shaded), during SON from 1979 to 2005 between ERA-Interim and (Figures 8a and 8c) small and (Figures 8b and 8d) large bias ensembles. Contour interval is 1 hPa for mslp and 10 m (black) and 100 m (shaded) for eddy geopotential height. The zero contour is omitted.

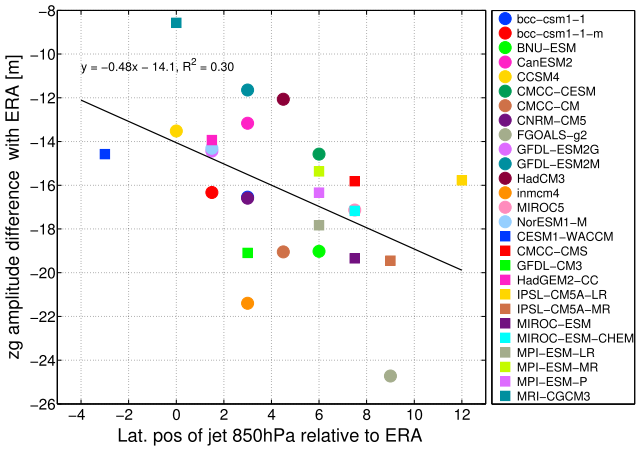


**Figure 9.** CMIP5 high-latitude 500 hPa eddy geopotential height amplitude bias relative to ERA-Interim versus bias in SH tropospheric jet at 850 hPa relative to ERA-Interim during SON. See section 4.2 for explanation of how each quantity was calculated. Circles represent low-top CMIP5 models, and squares represent high-top CMIP5 models. A linear fit is added, along with its regression coefficients and the $R^2$ value.

### 4.2. Representation of Links to Troposphere

In this section we explore whether model biases in high-latitude stratospheric heat flux extremes are connected to the tropospheric circulation in CMIP5 models. In the NH biases in stratospheric eddy heat flux were largest for extreme negative events, and this led to model biases in the North Atlantic jet stream and geopotential height. An important difference between the SH and NH is that the modeled mslp and eddy geopotential height exhibit large climatological biases compared to ERA-Interim. Figure 8 shows the difference between the CMIP5 models and ERA-Interim SON climatological mslp (a and b) and climatological eddy geopotential height (c and d), at 500 hPa (black) and 10 hPa (shaded). Individual models cannot capture the longitudinal position seasonal cycle of the ASL, and the central pressure is high compared to reanalysis [*Hosking et al.*, 2013]. Only the small bias models are able to capture the wave 1 high-latitude pattern at 10 hPa. Neither of the model ensembles are able to replicate the 500 hPa ERA-Interim SON climatology (Figure 4a and 4d) sufficiently, with the differences as large as between the model ensembles themselves. Since the mean state of the models are so biased, compared to ERA-Interim, we cannot use the CMIP5 models to detect the impact of biased stratospheric wave 1 heat flux extremes (Figure 5 on the mean tropospheric climate in the SH, in contrast to the NH.

We find that the biased eddy geopotential height variance at 500 hPa ($\sqrt{\overline{z'^2}}$) is significantly correlated with the position of the jet stream relative to reanalysis (defined as the difference in latitude of maximum zonal-mean zonal wind at 850 hPa) as shown in Figure 9. The biased position of the SH jet is well known [*Kidston and Gerber*, 2010]. The correlation coefficient is $r = -0.54$, and a linear regression explains 30% of the model variance. This suggests that reducing the bias in geopotential height is important.

The link between the representation of stratospheric heat flux extremes in CMIP5 historical simulations to tropospheric conditions can be quantified after removing the biased climatalogical mean state. Figure 10 compares the mslp anomaly of the small bias and large bias model ensembles with ERA-Interim. The small bias models are able to capture the strength and position of the anomalous mslp seen during the extreme events whereas the large bias models are unable to replicate this tropospheric variability. We obtain similar results for 500 hPa geopotential height and 850 hPa temperature (not shown). The issue of differences in the length of time series, with considerably fewer extreme days for large bias compared with small bias models, is discussed in Appendix A.

The large bias models do not capture the anomalous mslp over the Antarctic Peninsula during stratospheric extreme events. Figure 11 shows the SON distribution of anomalous daily mslp over the Antarctic Peninsula for ERA-Interim and the CMIP5 model ensembles. The region 60°–75°S, 240°–330°E was chosen to coincide with the center of the wave 1 anomalous pattern seen in Figures 3a and 3b. The large bias models (unlike the

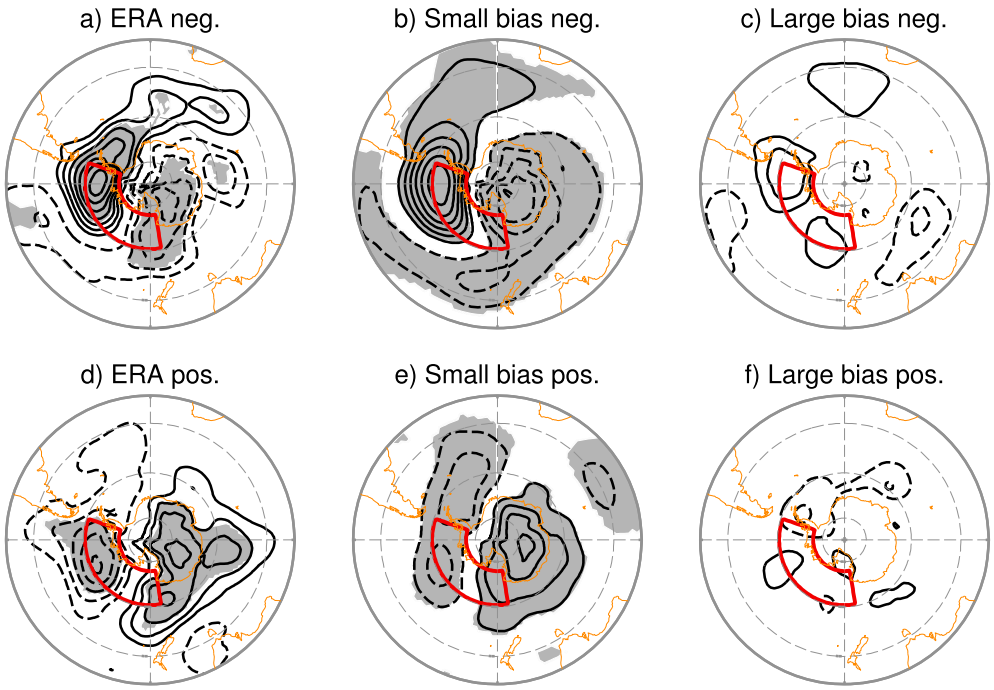


**Figure 10.** Mean sea level pressure field for extreme (a–c) negative days and extreme (d–f) positive days during 1979 to 2005. See section 3 for definition of extreme event days. The anomalies found for (Figures 10a and 10b) ERA-Interim are compared with those for the (Figures 10b and 10e) small bias model set and the (Figures 10c and 10f) large bias model set. Positive anomalies are shown with full lines, and negative anomalies are indicated by dashed lines, with contour levels of 10 m. The zero contour has been omitted in all plots. Grey shading shows anomalous values statistically significant at 99% (see Appendix A for details).

small bias models) do not capture the extent of the variability seen in reanalysis. In particular, the large bias ensemble distribution is significantly different from the ERA-Interim distribution at 99% significance according to a random sampling Kolmogorov-Smirnov test. The mean and variability of the small bias models agree well with ERA-Interim. Although the topography of the region makes the comparison harder, similar assertions can be made for eastern Antarctica. The representation of stratospheric wave events appears to be an important factor in the variability of Antarctic weather and climate patterns during spring.

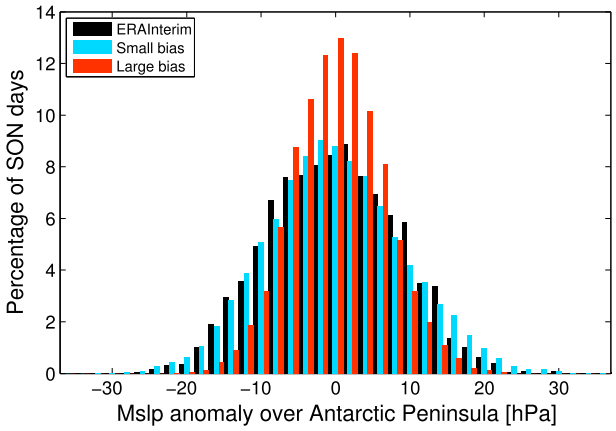


**Figure 11.** Daily distribution of anomalous mean sea level pressure averaged from 60°–75°S, 240°–330°E during SON from 1979 to 2005 for ERA-Interim (black) and small (blue) and large (red) bias CMIP5 model ensembles, with ensembles defined in Table 2.

## 5. Summary and Discussion

### 5.1. Summary

A dynamical metric of troposphere-stratospheric planetary wave heat flux events, defined as the 10th and 90th percentiles of the daily 50 hPa wave 1 heat flux originally developed for the NH, is applied to the SH. These extreme events in the stratosphere are associated with upward and downward wave coupling between the troposphere and the stratosphere. To investigate which CMIP5 models have realistic troposphere-stratosphere coupling in the SH, a small bias and a large bias ensemble are created containing models which can and cannot replicate the stratospheric heat flux extremes seen in ERA-Interim data, respectively. The main findings of this study on SH stratosphere-troposphere coupling are as follows:

1. In reanalysis, SH stratospheric heat flux extremes are linked to high-latitude tropospheric anomalies in the Amundsen Sea region. During extreme negative (positive) events there is a westward (eastward) shift of the ASL, a warming (cooling) and increase (decrease) of geopotential height over the Amundsen and Bellingshausen Seas. These findings complement those from the NH where the largest impacts occurred in the North Atlantic [*Shaw and Perlwitz*, 2013, S14].
2. CMIP5 models exhibit a large climatological eddy geopotential height bias during SON which is connected to the well-known bias of the jet position. This climatological bias prevents an assessment of any potential impact of stratospheric heat flux extremes on tropospheric climate.
3. The impact of stratospheric heat flux extremes on tropospheric variability can be assessed after the climatological bias is removed. The results show that CMIP5 models with biased stratospheric heat flux extremes significantly underestimate mslp variability over the Antarctic Peninsula.

### 5.2. Discussion

We have demonstrated that stratospheric variability is linked to tropospheric variability over the ASL. However, large climatalogical mean biases in the SH circulation [*Kidston and Gerber*, 2010; *Ceppi et al.*, 2012; *Bracegirdle et al.*, 2013] mask any impact of troposphere-stratosphere coupling on the tropospheric mean state.

We investigated potential sources of tropospheric bias including biased sea surface temperature and model resolution. However, we found no significant difference between the eddy geopotential height simulated in atmosphere-only models, AMIP (Atmospheric Model Intercomparison Project), and CMIP models. There are, however, a limited number of models available with AMIP runs so the size of the ensembles were restricted to two models in this analysis. We also found no relationship between the model bias and model resolution across CMIP5 models.

The distribution of Antarctic sea ice has been shown to influence the tropospheric circulation at high latitudes [*Raphael*, 2001]. The link to extreme changes in sea ice can be seen in mslp [*Wu et al.*, 1996] and 500 hPa geopotential height [*Renwick*, 2001]. Sea ice variability has a large radiative effect, as well as an impact on mass flux in the polar region [*Budd*, 1991].

Ozone has had a significant impact on regional climate in the SH during 1979–2005 [*Thompson and Solomon*, 2002]. There have been no significant changes in the 50 hPa heat flux distributions during SON; however, there are impacts later in the seasonal cycle [*Shaw et al.*, 2011]. How troposphere-stratosphere coupling in the SH will change during the period of ozone recovery is a question for further research.

We have shown that planetary wave coupling is linked to climate variability of the Amundsen Sea region. The vast majority of coupled climate models are not reproducing the observed trends in Antarctic sea ice extent [*Arzel et al.*, 2006; *Eisenman et al.*, 2011; *Maksym et al.*, 2012; *Turner et al.*, 2013b], so improving simulation of Antarctic climate variability and connections to the ASL is an important question for future research [*Raphael et al.*, 2015]. Our results suggest an accurate simulation of stratospheric variability is important for the ASL. Understanding the dynamical mechanism responsible for the link between troposphere-stratosphere planetary-scale wave coupling and the ASL and Antarctic tropospheric climate variability is an area for future research.

## Appendix A: Statistical Significance of Anomalous Values

The grey shading in Figures 3 and 10 indicates that the anomalous values are statistically significant at 99%. This analysis was completed, for every latitude and longitude grid point, by taking 10,000 random composite subsamples, with each subsample the same size as the composite of extreme events, from the whole SON

time series to create a distribution. The shaded areas occur outside of the 0.5th and 99.5th percentile of this distribution and so can be thought of as statistically distinct from the natural variability of the region. This also solves the issue of differing length of time series and uses the entire period of data available.

**Acknowledgments**
The authors thank K. Smith for helpful discussions on the manuscript. This research was supported by the National Science Foundation under grant AGS-1129519. The authors are grateful to three anonymous reviewers whose comments helped improve the manuscript. We thank Haibo Liu and the Lamont-Doherty Earth Observatory for obtaining the CMIP5 data and the World Climate Research Programmes Working Group on Coupled Modelling, which is responsible for CMIP. We also thank the climate modeling groups for producing and making available their model output. For CMIP the U.S. Department of Energy's Program for Climate Model Diagnosis and Intercomparison provides coordinating support and led development of software infrastructure in partnership with the Global Organization for Earth System Science Portals. The CMIP data used in this paper are available at http://cmip-pcmdi.llnl.gov/cmip5/data_portal.html. We also thank the ECMWF for providing the ERA-Interim reanalysis data set. The ERA-Interim data used in this paper are available at http://data-portal.ecmwf.int/data/d/interim_daily/levtype=pl/. The work of T.A.S. is supported by the National Science Foundation under the grant AGS-1129519. The work of L.M.P. and M.R.E. is funded by "Frontiers of Earth Systems Dynamics" grant from the U.S. National Science Foundation.

## References

Andrews, D., J. Holton, and C. Leovy (1987), *Middle Atmosphere Dynamics, International Geopyhsics Series*, vol. 40, Academic Press, London.
Arzel, O., T. Fichefet, and H. Goosse (2006), Sea ice evolution over the 20th and 21st centuries as simulated by current AOGCMs, *Ocean Model.*, *12*, 401–415, doi:10.1016/j.ocemod.2005.08.002.
Baines, P., and K. Fraedrich (1989), Topographic effects on the mean tropospheric flow patterns around Antarctica, *J. Atmos. Sci.*, *46*(22), 3401–3415, doi:10.1175/1520-0469(1989)046<3401:TEOTMT>2.0.CO;2.
Baldwin, M., and T. Dunkerton (2001), Stratospheric harbingers of anomalous weather regimes, *Science*, *294*, 581–584, doi:10.1126/science.1063315.
Baldwin, M., D. Stephenson, D. Thompson, T. Dunkerton, A. Charlton, and A. O'Neil (2003), Stratospheric memory and skill of extended-range weather forecasts, *Science*, *301*, 636–640, doi:10.1126/science.1087143.
Boville, B., and X. Cheng (1988), Upper boundary effects in a general circulation model, *J. Atmos. Sci.*, *45*(18), 2591–2606, doi:10.1175/1520-0469(1988)045<2591:UBEIAG>2.0.CO;2.
Bracegirdle, T., E. Suckburgh, J. Salee, Z. Wang, A. Meijers, N. Bruneau, T. Phillips, and L. Wilcox (2013), Assessment of surface winds over the Atlantic, Indian and Pacific Ocean sectors of the Southern Ocean in CMIP5 models: Historical bias, forcing response and state dependence, *J. Geophys. Res. Atmos.*, *118*, 547–562, doi:10.1002/jgrd.50153.
Budd, W. (1991), Antarctica and global change, *Clim. Change*, *18*, 271–299.
Ceppi, P., Y. Hwang, D. Frierson, and D. Hartmann (2012), SH jet latitude biases in CMIP5 models linked to shortwave cloud forcings, *Geophs. Res. Lett.*, *39*, L19708, doi:10.1029/2012GL053115.
Charlton-Perez, A., et al. (2013), On the lack of stratospheric dynamical variability in low-top versions of the CMIP5 models, *J. Geophys. Res. Atmos.*, *118*, 2494–2505, doi:10.1002/jgrd.50125.
Charney, J., and P. Drazin (1961), Propagation of planetary-scale disturbances from the lower into the upper atmosphere, *J. Geophys. Res.*, *66*(1), 83–109, doi:10.1029/JZ066i001p00083.
Dee, D., et al. (2011), The ERA-Interim reanalysis: Configuration and performance of the data assimilation system, *Q. J. R. Meteorol. Soc.*, *137*, 553–597.
Dunn-Sigouin, E., and T. Shaw (2015), Comparing and contrasting extreme stratospheric events, including their coupling to the tropospheric circulation, *J. Geophys. Res. Atmos.*, *120*, 1374–1390, doi:10.1002/2014JD022116.
Eisenman, I., T. Schneider, D. Battisti, and C. Bitz (2011), Consistent changes in the sea ice seasonal cycle in response to global warming, *J. Clim.*, *24*, 5325–5335, doi:10.1175/2011JCLI4051.1.
Fogt, R., A. Wovrosh, R. Langen, and I. Simmonds (2012), The characteristic variability and connection to the underlying synoptic activity of the Amundsen-Bellingshausen Seas Low, *J. Geophys. Res.*, *117*, D07111, doi:10.1029/2011JD017337.
Gerber, E., et al. (2012), Understanding the impact of stratospheric dynamics and variability on the Earth system, *Bull. Am. Meteorol. Soc.*, *93*(6), 845–859, doi:10.1175/BAMS-D-11-00145.1.
Harnik, N., J. Perlwitz, and T. Shaw (2011), Observed decadal change in downward wave coupling between the stratosphere and troposphere in the Southern Hemisphere, *J. Clim.*, *24*, 4558–4569, doi:10.1175/2011JCLI4118.1.
Hosking, J., A. Orr, G. Marshall, J. Turner, and T. Phillips (2013), The influence of the Amundsen Sea Low on the climate of West Antarctica and its representation in coupled climate model simulations, *J. Clim.*, *26*, 6633–6648, doi:10.1175/JCLI-D-12-00813.1.
Kidston, J., and E. Gerber (2010), Intermodel variability of the poleward shift of the austral jet stream in the CMIP3 integrations linked to biases in 20th century climatology, *Geophys. Res. Lett.*, *37*, L09708, doi:10.1029/2010GL042873.
Kidston, J., A. Scaife, S. Hardiman, D. Mitchell, N. Butchart, M. Baldwin, and L. Gray (2015), Stratospheric influence on tropospheric jet streams, storm tracks and surface weather, *Nat. Geosci.*, *8*, 433–440, doi:10.1038/ngeo2424.
Maksym, T., S. Stammerjohn, S. Ackley, and R. Massom (2012), Antarctic sea ice—A polar opposite?, *Oceanography*, *25*(3), 140–151, doi:10.5670/oceanog.2012.88.
Plumb, A. (2010), *Planetary Waves*, AGU, Washington, D. C.
Polvani, L., and D. Waugh (2004), Upward wave activity flux as a precursor to extreme stratospheric events and subsequent anomalous surface weather regimes, *J. Clim.*, *17*, 3548–3554.
Randel, W. (1987), A study of planetary waves in the southern winter troposphere and stratosphere. Part I: Wave structure and vertical propagation, *J. Atmos. Sci.*, *44*(6), 917–935, doi:10.1175/1520-0469(1987)044<0936:ASOPWI>2.0.CO;2.
Randel, W. (1988), The seasonal evolution of planetary waves in the SH stratosphere and troposphere, *Q. J. R. Meteorol. Soc.*, *114*, 1385–1409, doi:10.1002/qj.49711448403.
Raphael, M. (2001), Response of the large-scale, Southern Hemisphere extratropical atmospheric circulation to extremes of Antarctic sea ice concentration in general circulation model, *Polar Geog.*, *25*(3), 218–238, doi:10.1080/10889370109377714.
Raphael, M., G. Marshall, J. Turner, R. Fogt, D. Schneider, D. Dixon, J. Hosking, J. Jones, and W. Hobbs (2015), The Amundsen Sea Low: Variability, change and impact on Antarctic climate, *Bull. Am. Meteorol. Soc.*, *97*, 111–121, doi:10.1175/BAMS-D-14-00018.1.
Renwick, J. (2001), Southern Hemisphere circulation and relations with sea ice and sea surface temperature, *J. Clim.*, *15*, 3058–3068.
Shaw, T., and J. Perlwitz (2010), The impact of stratospheric model configuration on planetary scale waves in Northern Hemisphere winter, *J. Clim.*, *23*, 3369–3389, doi:10.1175/2010JCLI3438.1.
Shaw, T., J. Perlwitz, and N. Harnik (2010), Downward wave coupling between the stratosphere and troposphere: The importance of meridional wave guiding and comparison with zonal-mean coupling, *J. Clim.*, *23*, 6365–6381, doi:10.1175/2010JCLI3804.1.
Shaw, T., and J. Perlwitz (2013), The life cycle of Northern Hemisphere downward wave coupling between the stratosphere and troposphere, *J. Clim.*, *26*, 1745–1763, doi:10.1175/JCLI-D-12-00251.1.
Shaw, T., J. Perlwitz, N. Harnik, P. Newman, and S. Pawson (2011), The impact of stratospheric ozone changes on downward wave coupling in the Southern Hemisphere, *J. Clim.*, *24*, 4210–4229, doi:10.1175/2011JCLI4170.1.
Shaw, T., J. Perlwitz, and O. Weiner (2014), Troposphere-stratosphere coupling: Links to North Atlantic weather and climate, including their representation in CMIP5 models, *J. Geophys. Res.*, *119*, 5864–5880, doi:10.1002/2013JD021191.
Taylor, K., R. Stouffer, and G. Meehl (2012), Overview of CMIP5 and the experiment design, *Bull. Am. Meteorol. Soc.*, *93*, 485–498, doi:10.1175/BAMS-D-11-00094.1.

Thompson, D., and S. Solomon (2002), Interpretation of recent Southern Hemisphere climate change, *Science*, *296*, 895–899, doi:10.1126/science.1069270.

Turner, J., S. Colwell, and S. Harangozo (1997), Variability of precipitation over the coastal western Antarctic Peninsula from synoptic observations, *J. Geophys. Res.*, *102*(D12), 13,999–14,007.

Turner, J., T. Phillips, J. Hosking, G. Marshall, and A. Orr (2013a), The Amundsen Sea Low, *Int. J. Climatol.*, *33*, 1818–1829, doi:10.1002/joc.3558.

Turner, J., T. Bracegirdle, T. Phillips, G. Marshall, and J. Hosking (2013b), An initial assessment of Antarctic sea ice extent in the CMIP5 models, *J. Clim.*, *26*, 1473–1484, doi:10.1175/JCLI-D-12-00068.1.

van Loon, H., and R. Jenne (1972), The zonal harmonic standing waves in the Southern Hemisphere, *J. Geophys. Res.*, *77*(6), 992–1003.

Walsh, K., I. Simmonds, and M. Collier (2000), Sigma-coordinate calculation of topographically forced baroclinicity around Antarctica, *Dynam. Atmos. Ocean*, *33*, 1–29.

Wu, X., I. Simmonds, and W. Budd (1996), Southern Hemisphere climate system recovery from instantaneous sea-ice removal, *Q. J. R. Meteorol. Soc.*, *122*, 1501–1520.